Hindawi
Shock and Vibration
Volume 2022, Article ID 7842921, 19 pages
https://doi.org/10.1155/2022/7842921

*Research Article*

# Study on Pressure Relief Technology of High-Pressure Water Jet of Residual Coal Pillar in Overlying Goaf in Close Seam Mining

**Shang Yang,[1] Xuehui Li,[2] Jun Wang,[1,3] Shuhao Yang,[1] Zhen Shen,[1] and Guangzheng Xu[1]**

[1]*College of Energy and Mining Engineering, Shandong University of Science and Technology, Qingdao 266590, China*
[2]*College of Transportation, Shandong University of Science and Technology, Qingdao 266590, China*
[3]*State Key Laboratory of Mining Disaster Prevention and Control, Shandong University of Science and Technology, Qingdao 266590, China*

Correspondence should be addressed to Xuehui Li; huizi6062@126.com and Jun Wang; wangjunsdkjd@126.com

Received 27 May 2021; Revised 11 November 2021; Accepted 3 December 2021; Published 13 January 2022

Academic Editor: Jianwei Cheng



To solve the problem of strong ground pressure behaviour under a residual coal pillar in the overlying goaf of a close-distance coal seam, this paper proposes the technology of weakening and relieving the residual coal pillar in the overlying goaf by a high-pressure water jet. Based on the geological occurrence of the No. 3 coal seam and mountain No. 4 coal seam in the Yanzishan coal mine, the high-pressure water jet pressure relief technology of residual coal pillars in the overlying goaf of close-distance coal seams was studied by theoretical analysis and field industrial tests. First, the elastic-plastic zone of the residual coal pillar and the stress distribution law of the floor are obtained by theoretical analysis, and the influence degree of the residual coal pillar on the support of the lower coal seam working face is revealed. Then, a high-pressure water jet combined with mine pressure is proposed to weaken the residual coal pillar. Finally, through the residual coal pillar hydraulic cutting mechanical model and "double-drilling double-slot" model, the high-pressure water jet drilling layout parameters are determined, and an industrial field test is carried out. The single knife cutting coal output and 38216 working face hydraulic support monitoring data show that high-pressure hydraulic slotting can weaken the strength of the coal body to a certain extent, destroy the integrity of the residual coal pillar, cut off the load transmission path of the overlying strata, and reduce the working resistance of the hydraulic support under the residual coal pillar to a certain extent, which is beneficial to the safe mining of the working face.

## 1. Introduction

In recent years, with the increase in coal mining intensity and mining depth, the occurrence conditions of coal seams have become more complex, the mining environment has worsened, and underground engineering disasters have become prominent [1–3]. For close-distance coal seam mining, the working face under the residual coal pillar in an overlying goaf is affected not only by the mining stress and tectonic stress but also by the residual coal pillar stress transmission, which makes the underground pressure behaviour of the lower coal seam working face more intense, and the support safety valve frequently opens, which seriously hinders the safe and efficient production by coal mines [4–8].

At present, the measures used to address the problem of strong mine pressure behaviour under the residual coal pillar in an overlying goaf mainly include coal seam directional blasting [9] and hydraulic fracturing [10]. Through the above treatment methods, the overall structure of the coal body can be destroyed, the strength of the coal body can be weakened, the connection form of the rock structure can be changed, the stress distribution form of the floor of the residual coal pillar can be improved, and the purpose of stress concentration can be alleviated. The above methods have been widely used in China because the geological conditions of different mining zones are different, the effect is also different, and there are some disadvantages. For example, coal seam directional blasting [11] not only involves a large amount of drilling

construction and low efficiency but is also likely to ignite harmful gas in the goaf, which poses a certain hidden danger to safe and efficient mining in coal mines. Conventional hydraulic fracturing technology [12, 13] easily controls fracture propagation by the original in situ stress, expands along the direction perpendicular to the minimum principal stress, and easily forms a cracking "blank zone" on both sides of the fracture. At the same time, there are many secondary fractures in the remaining coal pillar, and the high-pressure water loss is fast; thus, it is not easy to form the residual coal pillar damaged by pressure. With the continuous innovation of high-pressure water jet technology and the continuous improvement of high-pressure water generating devices, high-pressure water jet weakening technology has been applied to the prevention of dynamic disasters, control of hard roof stability in coal mines, and low-permeability coal seam gas extraction in underground coal mines. Relevant scholars [14–16] have used high-pressure hydraulic slotting to relieve the gas pressure inside the coal seam and increase the permeability of the coal mass, which thus improves the gas drainage efficiency and eliminates the outburst risk. Some scholars [17, 18] have used theoretical analysis, numerical simulation, and other research methods to study the pressure relief mechanism of high-pressure hydraulic slotting on coal and rock. After hydraulic cutting in the coal seam, a fully unloaded area, a transition pressure-relief area, and the original stress area are formed around the slot. After high-pressure hydraulic slotting in the roof, the strength of the roof is weakened, and the roof structure is changed, which can achieve the effect of unloading and releasing energy. Field practice has shown that high-pressure hydraulic slotting can reduce the stress load in the far and near fields and reduce the occurrence of dynamic disasters, such as rockburst and coal and gas outbursts.

In view of the mining conditions of carboniferous coal seams No. 3 and mountain No. 4 in the Yanzishan coal mine of the Datong Coal Mine Group, this paper adopts high-pressure water jet technology to weaken the residual coal pillar in the overlying goaf. First, the elastic-plastic zone of the residual coal pillar and the stress distribution law of floor are studied by theoretical analysis; the stress transfer mechanism of the overlying residual coal pillar floor in close proximity to coal seam downward mining is revealed; and then, based on theoretical analysis, numerical simulation, and field conditions, the drilling layout parameters of the high-pressure water jet destroying the residual coal pillar are determined. Finally, field industrial tests and effect inspections are carried out, and the research content of the paper can provide safety guarantees and theoretical guidance for the safe mining of close coal seams under similar conditions.

## 2. Engineering Geology

The 8216 working face of the No. 3 coal seam in the Yanzishan coal mine (hereinafter referred to as the 38216 working face) is located in the 302 panel of the No. 3 coal seam at the 910 level. The working face is 2540 m long and 180 m wide, with an average depth of 400 m, an average thickness of 5.0 m, and an average dip angle of 2°. In the east is the No. 3 layer panel roadway, in the south is the 8214 design working face of the No. 3 coal seam, in the west is the boundary of the No. 3 layer panel, and in the north is the 8218 design working face of the No. 3 coal seam. The upper part of the 38216 working face is the goaf of the 8216 working face and 8218 working face of the Mountain No. 4 coal seam (hereinafter referred to as the 48216 working face and 48218 working face), and the average spacing is 25 m. The residual coal pillar between the 48216 and 48218 working faces is located above the 38216 working face. The width of the coal pillar is 38 m. The coal pillar is 30 m from the 5216 roadway of the 38216 working face and 112 m from the 2216 roadway of the 38216 working face, as shown in Figure 1. The 5216 roadway is a tailgate with a size of 4.2 m × 3.4 m (width × height) and is supported by a "bolt-cable-mesh" framework, as shown in Figure 2(a). The 2216 roadway is a headgate with a size of 5.0 m × 3.3 m (width × height) and is supported by a "bolt-cable-mesh" framework, as shown in Figure 2(b). The distribution of roof and floor rocks is shown in Figure 3.

## 3. Elastic-Plastic Zone of the Residual Coal Pillar and the Stress Distribution Law of the Floor

Based on the mining conditions of working faces 38216, 48216, and 48218, theoretical analysis is used to study the failure characteristics and the stress distribution law of the residual coal pillar floor in the overlying goaf and reveal the influence degree of the residual coal pillar on the support of the lower coal seam working face.

*3.1. Elastic-Plastic Zone of the Residual Coal Pillar in the Overlying Goaf.* Analysis of mine pressure and strata control theory [19] showed that the residual coal pillar in the overlying goaf is deformed and damaged under the action of overlying strata pressure. Failure zone I, plastic zone II, and elastic zone III form from the outside to the inside, in which the elastic zone is the main bearing zone and the main medium for the downward transmission of the overlying load. In this part, combined with the mining conditions of the 48216 and 48218 working faces, and based on limit equilibrium theory [6], the elastic-plastic zone range of the residual coal pillar is analysed, and the elastic-plastic zone width of the residual coal pillar is obtained.

As shown in Figure 4, the structural model of the elastic-plastic zone of the residual coal pillar is presented. In the early stage of roadway excavation and the mining process of both sides of the working face, the section coal pillar is inevitably affected by mining, and the failure and plastic zones form at a certain width of the coal pillar edge. Based on limit equilibrium theory, the width of the elastic-plastic zone can be calculated:

$$B_0 = \frac{M}{2gf} \ln \frac{q_1 + c \cot \varphi}{g\left(p_1 + c \cot \varphi\right)}, \tag{1}$$

$$B_1 = B - 2B_0. \tag{2}$$

There $B$ is the width of the residual coal pillar, m; $B_0$ is the sum of the widths of the failure zone and plastic zone, m; $B_1$ is the width of the elastic zone, m; $M$ is the thickness of the coal seam, m; $q_1$ is the concentrated load above the residual

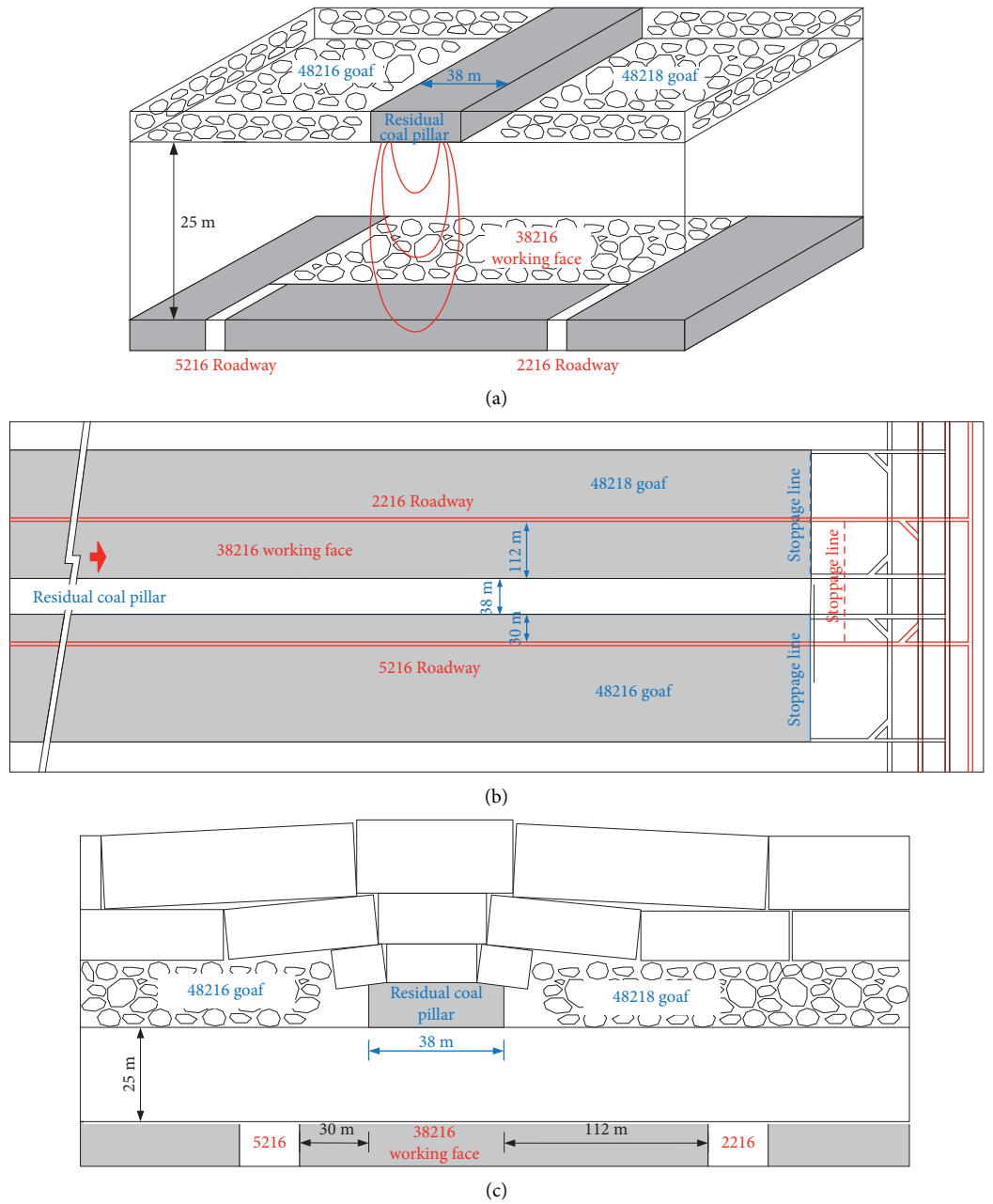


Figure 1: Spatial positional relationships between working faces. (a) Space location diagram. (b) Plane figure. (c) Section plan.

coal pillar, MPa; $c$ is the cohesion of coal, MPa; $\varphi$ is the angle of the internal friction of coal, °; $g$ is the triaxial stress coefficient, $g = (1 + \sin\varphi)/(1 - \sin\varphi)$; $f$ is the friction factor, $f = \tan\varphi$; and $p_1$ is the resistance of the support to the coal wall, MPa.

According to equation (1), the sum of the widths of the failure zone and plastic zone of the residual coal pillar $B_0$ calculated by limit equilibrium theory is related to the concentrated load above the coal pillar. According to mine pressure theory, the concentrated load above the overlying residual coal pillar $q_1$ is mainly caused by the weight of the overlying strata and the rotation of the cantilever beams on both sides of the pillar, as shown in Figure 5.

Due to the long mining time of the 48016 and 48218 working faces (mining completed in 2015-2016), the goaf on both sides of the residual coal pillar has been filled with overburden caving strata, and the overburden weight above the collapse line can be regarded as bearing by the gangue and residual coal pillar in the goaf, that is, the total load on the residual coal pillar $P$:

$$P = \left[BH + 2h(H - h)\tan\frac{\delta}{2} + h^2\tan\frac{\delta}{2}\right]\gamma. \quad (3)$$

There $H$ is the burial depth of the residual coal pillar, m; $h$ is the caving height of the strata in the goaf, m, where Yu [20]

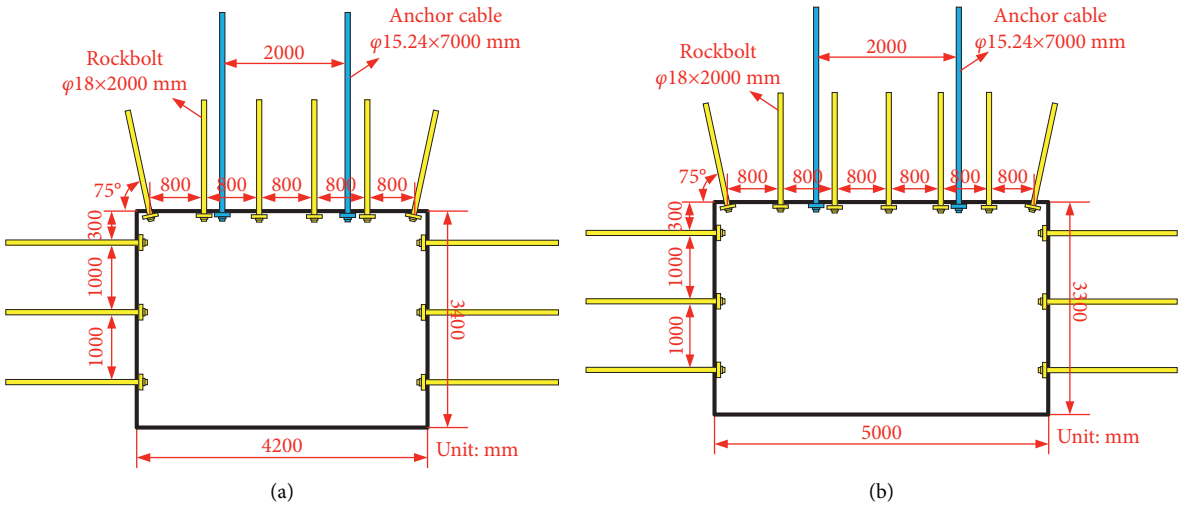


Figure 2: Support schemes of the roadway supports. (a) 5216 roadway. (b) 2216 roadway.

| Stratigraphic Columnar | Lithological Characters | Thickness (m) | Depth (m) |
|---|---|---|---|
| | Fine medium sandstone | 20 | 314 |
| | Medium sandstone | 15 | 329 |
| | Kaolin mudstone | 20 | 349 |
| | Sandy mudstone | 10 | 359 |
| | Siltstone | 10 | 369 |
| | Mountain No.4 coal seam | 6 | 375 |
| | Siltstone | 10 | 385 |
| | Medium grained sandstone | 10 | 395 |
| | Lamprophyre | 5 | 400 |
| | No.3 coal seam | 5 | 405 |
| | Sand mud interbedding | 9 | 414 |

Figure 3: Comprehensive drilling histogram.

found that the ratio of the caving height of the strata to the mining height is 10–12 in top-coal caving mining in the carboniferous system; $\delta$ is the caving angle of the overlying strata in the goaf, °, where according to the research of relevant scholars [21–23], the caving angle in the carboniferous system is generally 60°–63°; and $\gamma$ is the average unit weight of the overlying strata, kN/m$^3$.

Concentrated load above the residual coal pillar $q_1$ is

$$q_1 = \frac{P}{B} = \frac{\left[BH + 2h(H-h)\tan(\delta/2) + h^2\tan(\delta/2)\right]\gamma}{B}. \quad (4)$$

According to the geological conditions of the 48216 and 48218 working faces in the Mountain No. 4 coal seam of the Yanzishan coal mine, the following parameters can be determined: $B$ is 38 m, $H$ is 375 m, $h$ is 70 m, $\delta$ is 60°, and $\gamma$ is 26 kN/m$^3$. By substituting the above parameters into

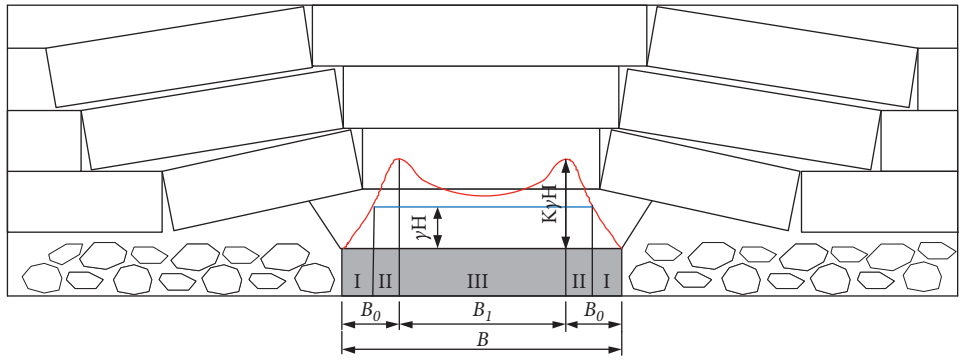


Figure 4: Structural model of the elastic-plastic zone of the residual coal pillar.

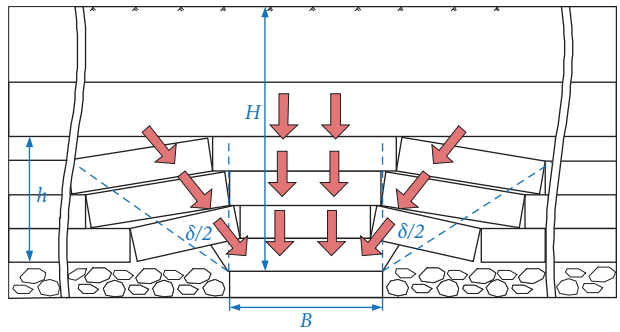


Figure 5: Calculation model of the concentrated load above the residual coal pillar.

equation (4), it can be concluded that the concentrated load above the residual coal pillar $q_1$ is 28.6 MPa.

According to the geological survey of the Mountain No. 4 coal seam, the coal seam thickness $M$ is 6 m, the concentrated load above the coal pillar $q_1$ is 28.6 MPa, the cohesion of coal $c$ is 1.76 MPa, the internal friction angle of coal $\varphi$ is 22°, the friction coefficient of the contact surface between the coal seam and the roof and floor $f$ is 0.4, and the resistance of the support to the coal wall $p_1$ is 0. By substituting the above parameters into equations (1) and (2), the sum of the width of the failure zone and plastic zone on one side of the residual coal pillar $B_0$ is approximately 4.2 m, and the elastic core zone $B_1$ is approximately 29.6 m.

*3.2. Stress Distribution Law of the Residual Coal Pillar Floor in the Overlying Goaf.* In close-distance coal seam mining, the lower coal seam working face is often located under the residual coal pillar in the overlying goaf. Because the overlying residual coal pillar plays a role in load transfer, it will form a complex stress environment around the working face of the lower coal seam, resulting in stress concentration, which seriously hinders safe and efficient production in coal mines. To understand the residual coal pillar floor stress size and distribution form in more detail, based on the theory of elasticity, the residual coal pillar and floor are simplified as an elastomer, and the residual coal pillar stress calculation model is established.

According to the analysis in Figure 6, the stress at any point $M$ in the half-plane caused by the small concentrated load $\mathrm{d}F = \lambda q d\xi$ is as follows:

$$\begin{cases} \mathrm{d}\sigma_x = \dfrac{2\lambda q\, d\xi}{\pi} \dfrac{x^3}{\left[x^2 + (y-\xi)^2\right]^2}, \\ \mathrm{d}\sigma_y = \dfrac{2\lambda q\, d\xi}{\pi} \dfrac{x(y-\xi)^2}{\left[x^2 + (y-\xi)^2\right]^2}, \\ \mathrm{d}\tau_{xy} = \dfrac{2\lambda q\, d\xi}{\pi} \dfrac{x^2(y-\xi)}{\left[x^2 + (y-\xi)^2\right]^2}. \end{cases} \tag{5}$$

To determine the stress caused by the uniformly distributed load acting on the residual coal pillar, it is necessary to superimpose the stress caused by each small concentrated load, and the integral of equation (5) is obtained:

$$\begin{cases} \sigma_x = \dfrac{2}{\pi} \displaystyle\int_{-a}^{b} \dfrac{\lambda q x^3 \mathrm{d}\xi}{\left[x^2 + (y-\xi)^2\right]^2}, \\ \sigma_y = \dfrac{2}{\pi} \displaystyle\int_{-a}^{b} \dfrac{\lambda q x (y-\xi)^2 \mathrm{d}\xi}{\left[x^2 + (y-\xi)^2\right]^2}, \\ \tau_{xy} = \dfrac{2}{\pi} \displaystyle\int_{-a}^{b} \dfrac{\lambda q x^2 (y-\xi) \mathrm{d}\xi}{\left[x^2 + (y-\xi)^2\right]^2}. \end{cases} \tag{6}$$

For the uniformly distributed load above the residual coal pillar, $\lambda_q$ is a constant, and the integral of equation (6) is obtained:

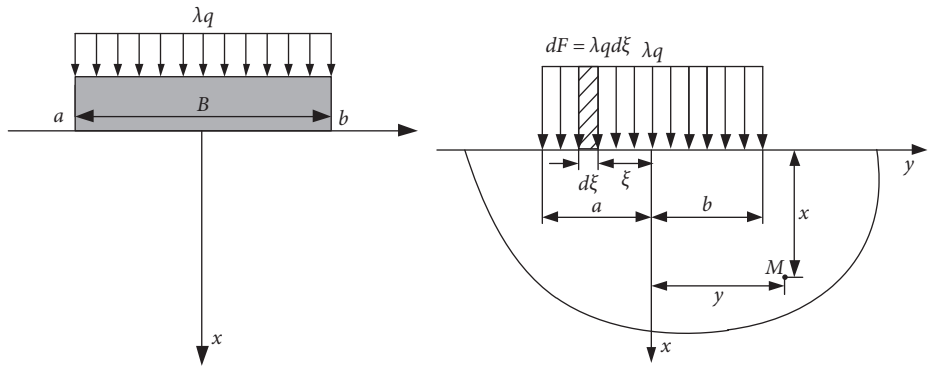


Figure 6: Stress calculation model of the residual coal pillar.

$$\begin{cases} \sigma_x = \dfrac{\lambda q}{\pi}\left[\arctan\dfrac{y+b}{x} - \arctan\dfrac{y-a}{x} + \dfrac{x(y+b)}{x^2+(y+b)^2} - \dfrac{x(y-a)}{x^2+(y-a)^2}\right], \\ \sigma_y = \dfrac{\lambda q}{\pi}\left[\arctan\dfrac{y+b}{x} - \arctan\dfrac{y-a}{x} - \dfrac{x(y+b)}{x^2+(y+b)^2} + \dfrac{x(y-a)}{x^2+(y-a)^2}\right], \\ \tau_{xy} = \dfrac{\lambda q}{\pi}\left[\dfrac{x^2}{x^2+(y+b)^2} - \dfrac{x^2}{x^2+(y-a)^2}\right]. \end{cases} \tag{7}$$

To better study the stress distribution law of the residual coal pillar floor in the overlying goaf, the mining conditions of the 48126 and 48128 working faces in the Yanzishan coal mine are taken as the research background, the stress of the residual coal pillar floor is analysed by equation (7), $\lambda q$ is a constant, and the distribution of horizontal stress, vertical stress, and shear stress at different depths of the residual coal pillar under uniform load are obtained by using Origin data processing software.

According to the analysis in Figure 7, the stress distribution law of the residual coal pillar floor is as follows:

(1) The vertical stress of the floor of the residual coal pillar is distributed as a whole in a "single-arch" pattern, which is distributed symmetrically in the centre of the coal pillar, and the peak values of the vertical stress occur at the central axis of the coal pillar. In the vertical direction, with increasing depth, the stress decreases; however, the range of stress influence expands, and the depth of the vertical stress concentration is approximately 60 m. In the horizontal direction, the stress decreases with increasing distance from the central axis of the coal pillar.

(2) The horizontal stress of the floor of the residual coal pillar is symmetrically distributed along the central axis of the coal pillar. In the vertical direction, as the depth increases, the whole stress changes from a single peak to a "double-arch" shape, the change trend of stress tends to ease, and the influence range of stress also expands. In the horizontal direction, the change trend is consistent with that in the vertical direction, and the stress decreases with the increase in the distance from the coal pillar central axis.

(3) The shear stress of the residual coal pillar floor has a "single peak" on one side. The shear stress value at the central axis of the coal pillar is 0. With increasing distance from the central axis of the coal pillar, the shear stress first increases and then decreases, and the stress peak is located at the edge of the coal pillar.

(4) According to the above analysis, the influence depth of the vertical stress of the residual coal pillar is 60 m, the influence depth of the horizontal stress is approximately 10 m, and the influence depth of the shear stress is small. Therefore, the vertical stress plays a leading role in the stress transfer process of the residual coal pillar floor.

According to the above analysis, the peak value of vertical stress in the floor of the residual coal pillar appears at the central axis of the coal pillar. According to the mining conditions of the 38216 working face, the 38216 working face is 25 m from the overlying residual coal pillar. According to Figure 7(a), at 25 m below the coal pillar, the stress concentration factor $\lambda$ is approximately 2.33, and the stress transferred by the residual coal pillar is approximately 22.7 MPa.

*3.3. Load-Bearing Capacity of the Working Face Support under the Residual Coal Pillar.* In this part, theoretical calculations are used to analyse the influence of residual coal pillars on the working face from a quantitative point of view. According to the theory of mine pressure and strata control, as the 38126 working face supports advance and load is transferred by the overlying roof, it also bears the

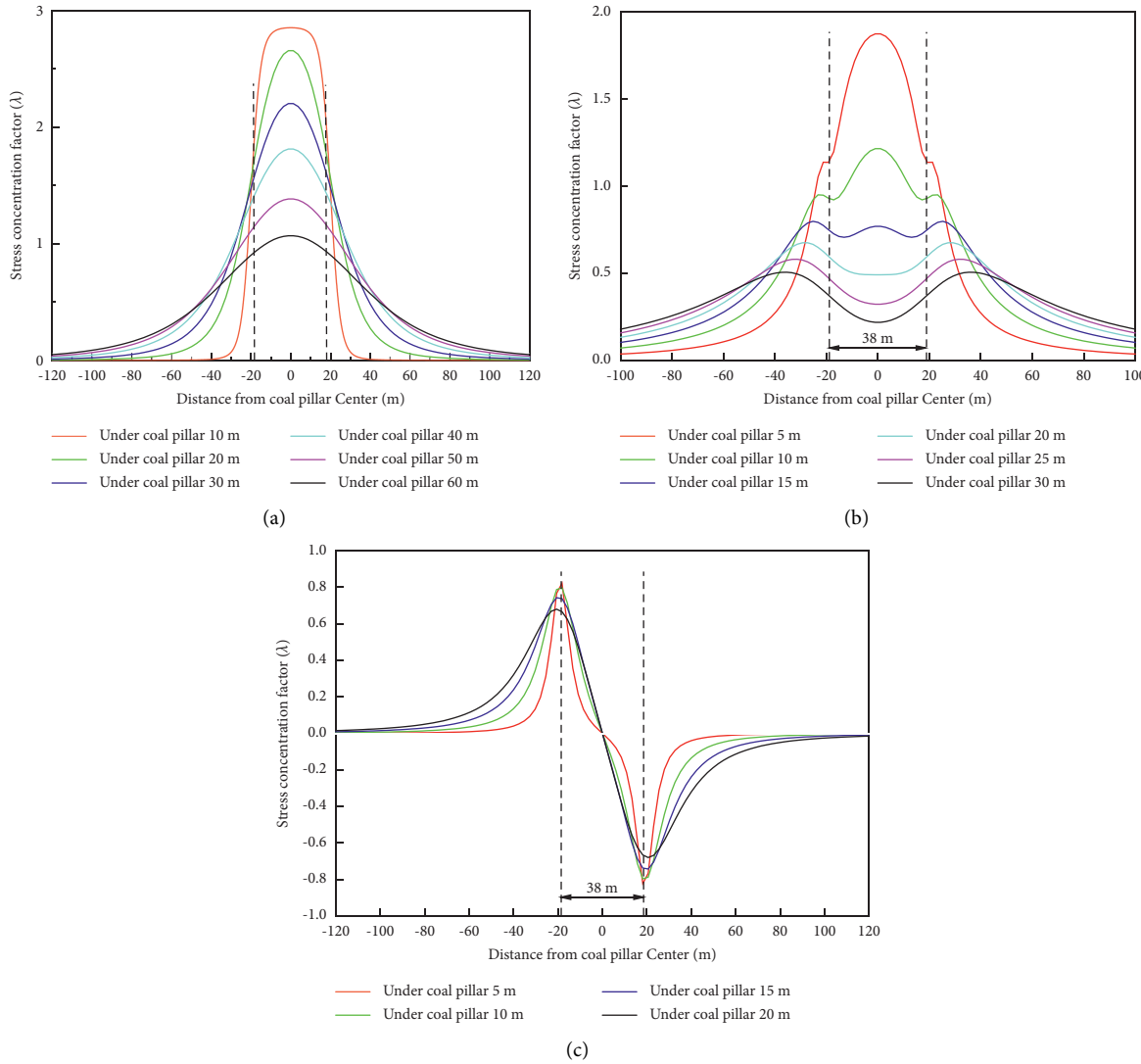


Figure 7: Stress distributions of the residual coal pillar floor at different depths. (a) Vertical stress. (b) Horizontal stress. (c) Shear stress.

concentrated load transferred by the overlying residual coal pillar. As shown in Figure 8, the working face under the residual coal pillar mainly bears the following loads:

$$P_m(n) = \frac{E_n H_n{}^3 \left(\gamma_n H_n + \gamma_{n+1} H_{n+1} + \gamma_{n+2} H_{n+2} + \cdots + \gamma_m H_m + \sigma_x\right)}{E_n H_n{}^3 + E_{n+1} H_{n+1}{}^3 + \cdots + E_m H_m{}^3}. \tag{8}$$

There $E_i$ is the elastic modulus of layer $i (i = n, n+1, \ldots, m)$ above the lower coal seam, MPa; $H_i$ is the thickness of the rock stratum of layer $i$ $(i = n, n+1, \ldots, m)$ above the lower coal seam, m; $\gamma_i$ is the volume force of the rock stratum of layer $I$ $(i = n, n+1, \ldots, m)$ above lower coal seam, MN/m$^3$; and $\sigma_x$ is the load transferred by the overlying residual coal pillar, MPa

According to the geological survey of the No. 3 coal seam and Mountain No. 4 coal seam, there are three rock strata between the 38216 working face and the 48216 and 48218 goafs: lamprophyre, medium-grained sandstone, and siltstone. The mechanical parameters of each rock stratum are shown in Table 1.

In addition, according to the previous theoretical analysis, the transfer load of the 38216 working face under the residual coal column is approximately 22.7. By substituting the above parameters into equation (8), the main load of the working face under the residual coal pillar is approximately 1.25 MPa, which is greater than the support strength of the hydraulic support (ZF12000/22/35). During the mining of the lower coal seam, it is easy to cause the working resistance of the hydraulic support under the residual coal pillar to be too large, and the safety valve is frequently opened, which may cause support crushing accidents.

According to the above research, after the upper coal seam is mined, the overlying strata break, rotate, and sink, and the generated load is transmitted downwards. A part of the load acts on the gangue in the goaf. Because the gangue in the goaf consumes and transfers part of the load in the compaction process, the load transferred from the gangue in the goaf to the floor is small. Part of the load is transmitted downward through the residual coal pillars and

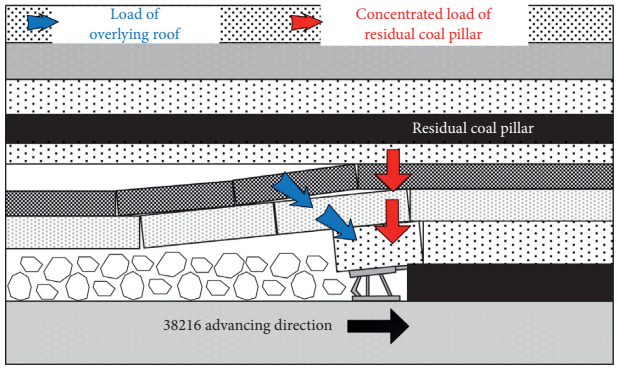


Figure 8: Structural model of the support bearing the load on the working face under a residual coal pillar.

distributes in the floor in the form of a "stress bubble," forming a stress concentration area, as shown in Figure 9. If the working face or roadway of the lower coal seam is located in the stress concentration zone, the pressure of the hydraulic support in the lower coal seam will increase, and the safety valve will be frequently opened. Roof subsidence, floor heave, and two sides moving close will occur in the roadway. This will seriously affect the safe mining of the lower coal seam.

## 4. Process Parameters of High-Pressure Water Jet Weakening the Residual Coal Pillar

*4.1. Pressure Relief Method of Weakening the Residual Coal Pillar by a High-Pressure Water Jet.* The width of the residual coal pillar in the goaf is a key factor affecting the size and distribution of the coal pillar floor stress. According to previous research results, the residual coal pillar deforms and is destroyed under the action of overlying pressure. From outside to inside, there are failure zone I, plastic zone II, and elastic core zone III. The elastic core zone is the main bearing area and the main medium for the downward transmission of the overlying load. Therefore, if the coal strength in the elastic core zone is artificially weakened, the integrity of the whole coal pillar will be reduced, the coal pillar will fail under the action of the overlying load, the load transmission path of the overlying strata will be cut off, and the lower close coal seam will be in the low-stress zone. Therefore, to improve the construction efficiency and reduce the construction cost, the idea of weakening residual coal pillars combined with applying a high-pressure water jet and mine pressure can be adopted. First, a high-pressure water jet is used to weaken the coal pillar and make the defect body in the elastic core to destroy the coal body around the defect body and reduce the integrity of the coal pillar; then, the whole coal pillar with defects is destroyed by using mine pressure. The load transfer form of the residual coal pillar before and after weakening is shown in Figure 10.

*4.2. Determination of High-Pressure Water Jet Drilling Layout Parameters.* The drilling layout parameters of high-pressure water jet mainly include the coal pillar width direction drilling layout parameters and coal pillar length direction drilling layout parameters. According to relevant research, when the spacing is too large, stress concentration easily occurs between the two boreholes, and the ideal failure effect cannot be achieved. When the spacing is too small, there will be a stress reduction zone between the two boreholes, which can achieve the ideal failure effect. However, with the increase in on-site construction quantities and construction time, considerable manpower and material resources are wasted [24]. Therefore, determining the reasonable drilling layout parameters of a high-pressure water jet can not only achieve the destruction effect of the residual coal pillar but also ensure construction progress.

*4.2.1. Determination of Coal Pillar Width Direction Drilling Layout Parameters.* According to the previous research results, the sum of the widths of the failure zone and plastic zone $B_0$ on one side of the residual coal pillar is approximately 4.2 m, and the elastic core zone $B_1$ is approximately 29.6 m, as shown in Figure 11(a). According to the above analysis, only when elastic core zone $B_1$ is damaged can the load transmitted by the floor be reduced. This is the scheme designed to destroy the elastic core zone of residual coal pillar $B_1$: elastic core zone $B_1$ is divided into four parts: high-pressure water jet destruction zones $B_{2\text{-}1}$ and $B_{2\text{-}2}$ and non-water jet destruction elastic core zones $B_{3\text{-}1}$ and $B_{3\text{-}2}$, as shown in Figure 11(b). First, a high-pressure water jet is used to destroy the coal body in zones $B_{2\text{-}1}$ and $B_{2\text{-}2}$, making it a plastic zone. The water jet damage zone loses its bearing capacity, and the overlying load is transferred to the non-water jet damage elastic core zones $B_{3\text{-}1}$ and $B_{3\text{-}2}$; if the remaining zones $B_{3\text{-}1}$ and $B_{3\text{-}2}$ reach a certain width (and can be regarded as a small coal pillar), plastic failure occurs under the action of mine pressure, the whole coal pillar is damaged, and the residual coal pillar loses its bearing capacity, as shown in Figure 11(c).

It is assumed that when the width of the coal pillar is B, the load above the residual coal pillar is $q_1$; when the width of the coal pillar is $B_{3\text{-}1} + B_{3\text{-}2}$, the load above the residual coal pillar is $q'$ ($q' > q_1$), as shown in Figure 11(b). To ensure the complete failure of the elastic core zone of the residual coal pillar, the maximum width of $B_{3\text{-}1} + B_{3\text{-}2}$ in plastic failure under the action of load $q'$ should be determined before the high-pressure water jet destroys $B_{2\text{-}1}$ and $B_{2\text{-}2}$. As shown in Figure 11(b), the widths of $B_{3\text{-}1}$ and $B_{3\text{-}2}$ are equal. Therefore, the maximum width of $B_{3\text{-}1} + B_{3\text{-}2}$ can be obtained only by determining the width of $B_{3\text{-}1}$ or $B_{3\text{-}2}$. Under the action of load $q'$, the width of plastic zone $q'$, $B_{3\text{-}1}$, or $B_{3\text{-}2}$ is as follows:

$$B_{3-1} \text{ or } B_{3-2} = \frac{M}{2gf} \ln \frac{q\prime + c \cot \varphi}{g(\tau + c \cot \varphi)}. \tag{9}$$

When $B_{2\text{-}1}$ and $B_{2\text{-}2}$ are destroyed, $B_{2\text{-}1}$ and $B_{2\text{-}2}$ coal become a plastic zone, the weight of overlying strata is shared by $B_{3\text{-}1}$, and $B_{3\text{-}2}$ the coal bodies, coal body after $B_{2\text{-}1}$ and $B_{2\text{-}2}$ failure and goaf gangue, and the concentrated load $q'$ on the coal body in the $B_{3\text{-}1}$ and $B_{3\text{-}2}$ zone is as follows:

Table 1: Mechanical parameters of interlayer strata.

| Rock stratum | Volumetric force $\gamma_i$ (MN/m$^3$) | Thickness $H_i$ (m) | Elastic modulus $E_i$ (MPa) |
|---|---|---|---|
| Lamprophyre | 0.0266 | 5 | $3.000 \times 10^4$ |
| Medium-grained sandstone | 0.0263 | 10 | $3.845 \times 10^4$ |
| Siltstone | 0.0262 | 10 | $2.800 \times 10^4$ |

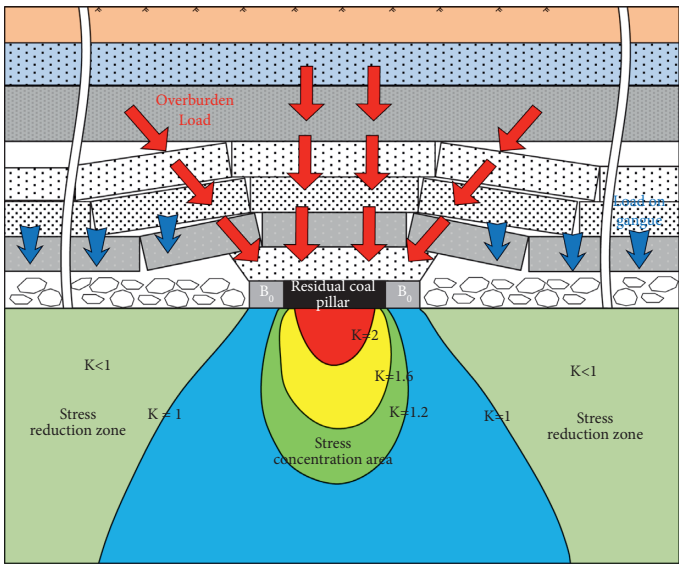


Figure 9: Transmission and distribution of the overlying load.

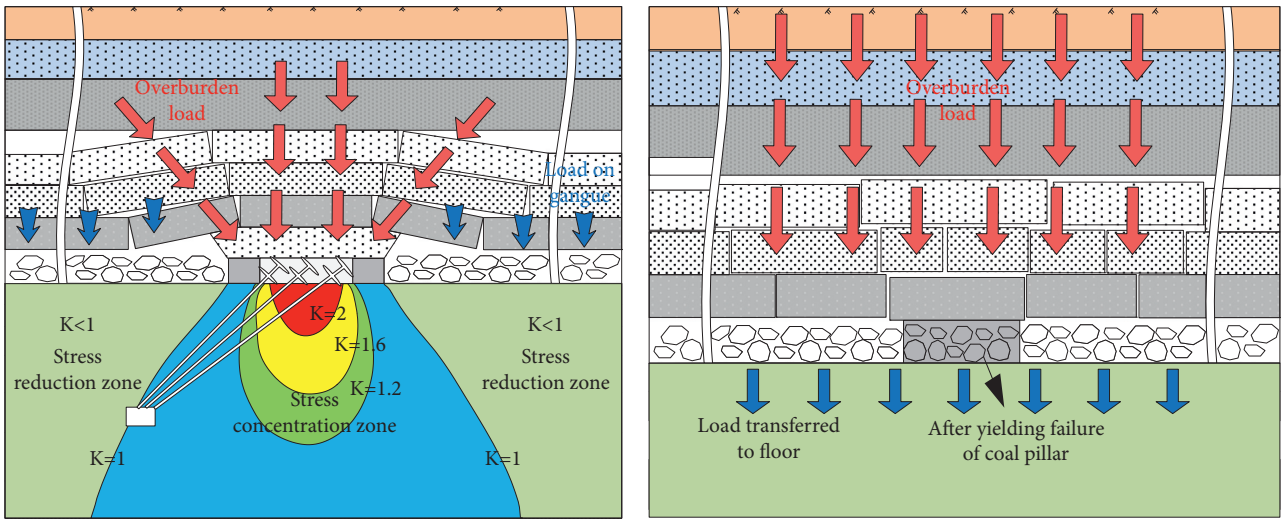


Figure 10: Load transfer before and after the weakening of the residual coal pillar. (a) Before weakening. (b) After weakening.

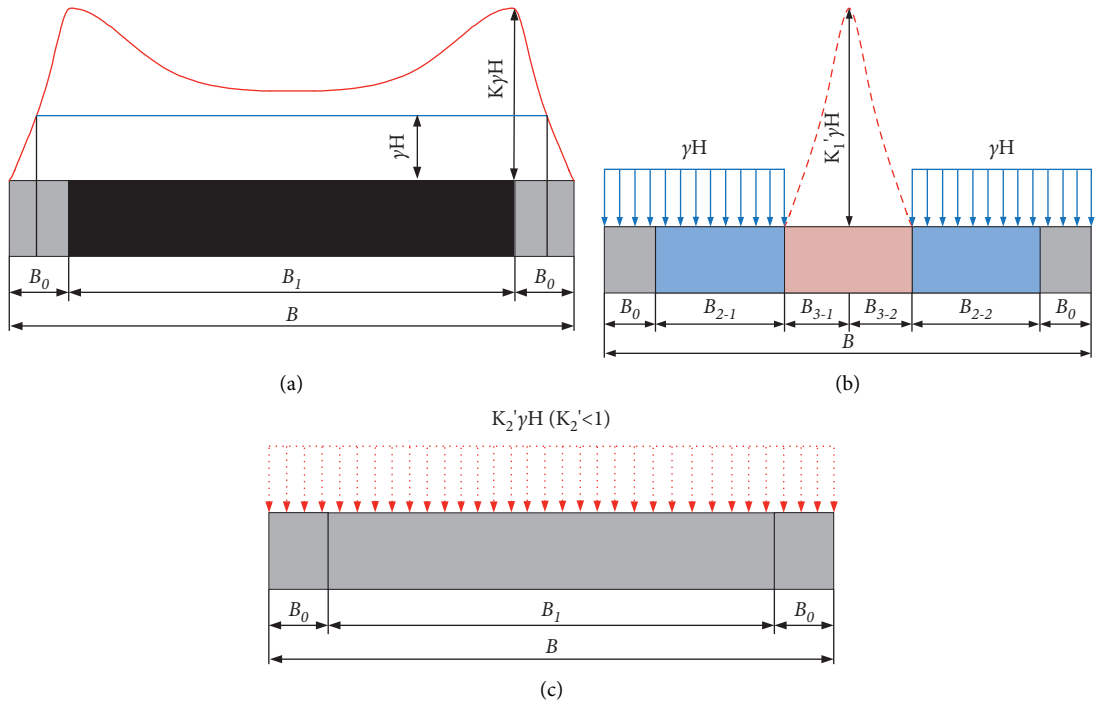


FIGURE 11: Mechanical model of the hydraulic cutting of the residual coal pillar. (a) Before coal pillar failure. (b) In the process of coal pillar failure. (c) After coal pillar failure.

$$q' = \frac{P'}{B_{3-1} + B_{3-2}} = \frac{\left[(B_{3-1} + B_{3-2})H + 2h(H-h)\tan(\delta/2) + h^2\tan(\delta/2)\right]\gamma}{B_{3-1} + B_{3-2}}. \tag{10}$$

When the overburden load acts on zones $B_{3\text{-}1}$ and $B_{3\text{-}2}$, zones $B_{3\text{-}1}$ and $B_{3\text{-}2}$ expand due to plastic failure. At this time, shear stress $\tau$ occurs on the interface of coal and rock in the $B_{2\text{-}1}$ and $B_{2\text{-}2}$ zones and acts on both sides of $B_{3\text{-}1}$ and $B_{3\text{-}2}$, as shown in Figure 11(b).

$$\tau = \gamma H \tan\varphi + c. \tag{11}$$

Substituting equations (10) and (11) into equation (9), we can obtain the following results:

$$B_{3-1} \text{ or } B_{3-2} = \frac{M}{2gf}\ln\frac{\left(\left[(B_{3-1} + B_{3-2})H + 2h(H-h)\tan(\delta/2) + h^2\tan(\delta/2)\right]\gamma/B_{3-1} + B_{3-2}\right) + c\cot\varphi}{g[\gamma H\tan\varphi + c(1+\cot\varphi)]}. \tag{12}$$

By substituting the above parameters (see Section 3.1 for details) into equation (12), $B_{3\text{-}1}$ can be obtained:

$$B_{3-1} = 3.378\ln\left(0.54 + \frac{13.8}{B_{3-1}}\right). \tag{13}$$

According to equation (13), $B_{3\text{-}1}$ is 4.4 m, and $B_{2\text{-}1}$ and $B_{2\text{-}2}$ are both 10.4 m. To ensure that the damage zone of the high-pressure water jet can be greater than 10.4 m, three boreholes are arranged in $B_{2\text{-}1}$ and $B_{2\text{-}2}$, and 2~3 slots are arranged in each borehole, with a slot spacing of 4 m, as shown in Figure 12. The borehole layout parameters are shown in Table 2.

*4.2.2. Determination of Coal Pillar Length Direction Drilling Layout Parameters.* In this part, FLAC 3D is used to study the influence of different drilling spacings in the length direction of the coal pillar on the stress field and plastic zone field of the coal body around the seam slot and determine the reasonable drilling spacing in the length direction of the coal pillar to provide a reference for on-site construction.

*(1) Establishment of the Model.* According to the research content of this part, the "double-drilling and double-slot" model is established, as shown in Figure 13. The model adopts the Mohr–Coulomb constitutive model. The model size is $X \times Y \times Z = (9\sim11)\text{ m} \times 15\text{ m} \times 10\text{ m}$, where the $x$-direction is the length direction of the coal pillar, the $y$-direction is the width direction of the coal pillar, and the $z$-direction is the vertical direction. The whole model is divided into three parts: drilling holes, slots, and surrounding coal bodies. The cylindrical shell grid is used for drilling holes and slots. To better study the damage, pressure relief effect, and

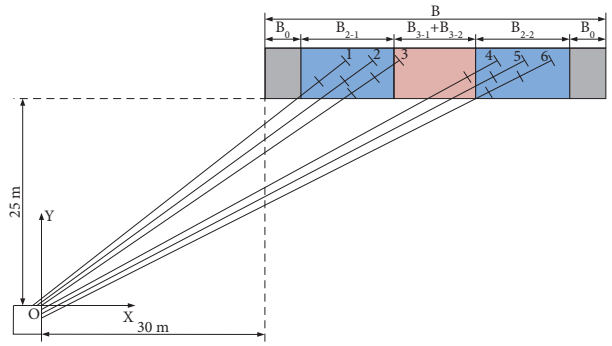


Figure 12: Coal pillar width direction drilling layout.

Table 2: Coal pillar width direction drilling layout parameters.

| Borehole number | Starting point of drilling | Azimuth of drilling (°) | Elevation angle of drilling (°) | Length of drilling hole (m) | Number of slots | Gap between slots (m) |
|---|---|---|---|---|---|---|
| 1 | (−1.0, 0) | 90 | 36 | 49.70 | 2 | 4 |
| 2 | (−0.5, 0) | 90 | 35 | 51.70 | 2 | 4 |
| 3 | (0, 0) | 90 | 33 | 53.80 | 3 | 4 |
| 4 | (0, 0.5) | 90 | 28 | 63.50 | 2 | 4 |
| 5 | (0, 1.0) | 90 | 27 | 66.40 | 2 | 4 |
| 6 | (0, 1.5) | 90 | 27 | 69.30 | 3 | 4 |

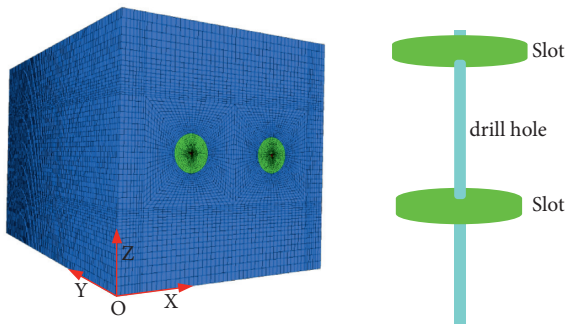


Figure 13: Double-drilling hole and double-slot model.

change law of coal bodies around drilling holes and slots, the division grid around drilling holes and slots is more dense. The surrounding coal body is a cylinder surrounded by a radial grid because it is far away from the borehole and fracture slot, and the division grid is relatively sparse. The model is divided into 945000~945600 units. According to Section 3.1, after the excavation of working faces 48216 and 48218 in the Mountain No. 4 coal seam, stress concentration occurs in the residual coal pillar, and the peak stress is 28.6 MPa. In this section, to ensure the accuracy and effectiveness of the simulation, a uniform load of 28.6 MPa is applied at the top of the model. The vertical displacement constraint is limited at the bottom of the model, and the horizontal displacement constraint is applied at the side. The physical and mechanical parameters of the model are shown in Table 3.

*(2) Simulation Scheme.* To better study the influence of different drilling spacings on the stress field and plastic zone field of coal around the slot, the drilling spacings in the length direction of the coal pillar are 3.0 m, 4.0 m, and 5.0 m, the slot radius is 0.75 m, the slot width is 0.2 m, and the slot spacing is 4 m.

To more intuitively understand the influence of different drilling spacings in the length direction of the coal pillar on the stress field and plastic zone field of the coal body around the slot, two observation sections are set: section 1 and section 2 (section 1 is parallel to the *xoz*-axis and passes through the slot section, as shown in Figure 14(a), while section 2 is parallel to the *xoy*-axis and passes through the borehole section, as shown in Figure 14(b)).

*(3) Analysis of Simulation Results*

(a) Vertical stress

(1) Section 1: as shown in Figure 15, a contour map of the vertical stress around the slot with different spacings in section 1 is shown. Figure 15 shows that with increasing drilling spacing, the stress value between drillings also increases, and a stress concentration area appears. When the distance between boreholes is 3 m, there is a stress overlap area between drillings, whose stress is less than the original rock stress, and it belongs to the stress reduction area. When the distance between drillings is 4 m, there is a stress concentration area between boreholes, the stress concentration value is 32 MPa, and the stress concentration degree is small. When the distance between drillings is 5 m, the stress concentration range between drillings increases, the stress concentration value also increases, reaching 42 MPa, and the stress concentration factor is 1.6.

(2) Section 2: as shown in Figure 16, a contour map of the vertical stress around the slot with

Table 3: Physical and mechanical parameters of the model.

| Rock stratum | Density (kg/m$^3$) | Bulk modulus (GPa) | Shear modulus (GPa) | Tensile strength (MPa) | Cohesion (MPa) | Internal friction angle (°) | Thickness (m) |
|---|---|---|---|---|---|---|---|
| Coal | 1410 | 2.1 | 1.3 | 1.50 | 1.76 | 22.00 | 6 |

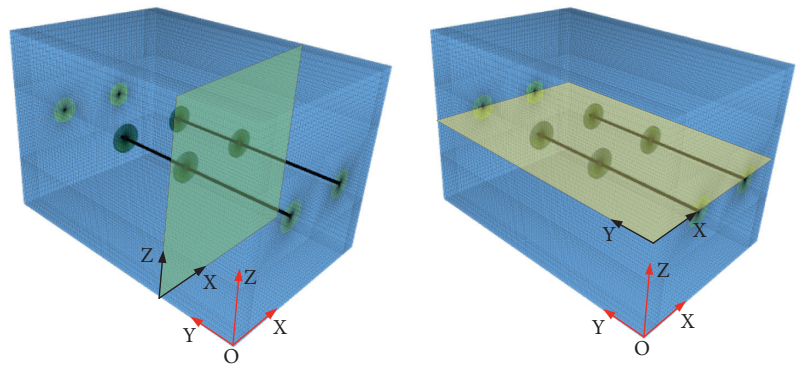


(a) (b)

Figure 14: Schematic diagram of the observation sections. (a) Section 1. (b) Section 2.

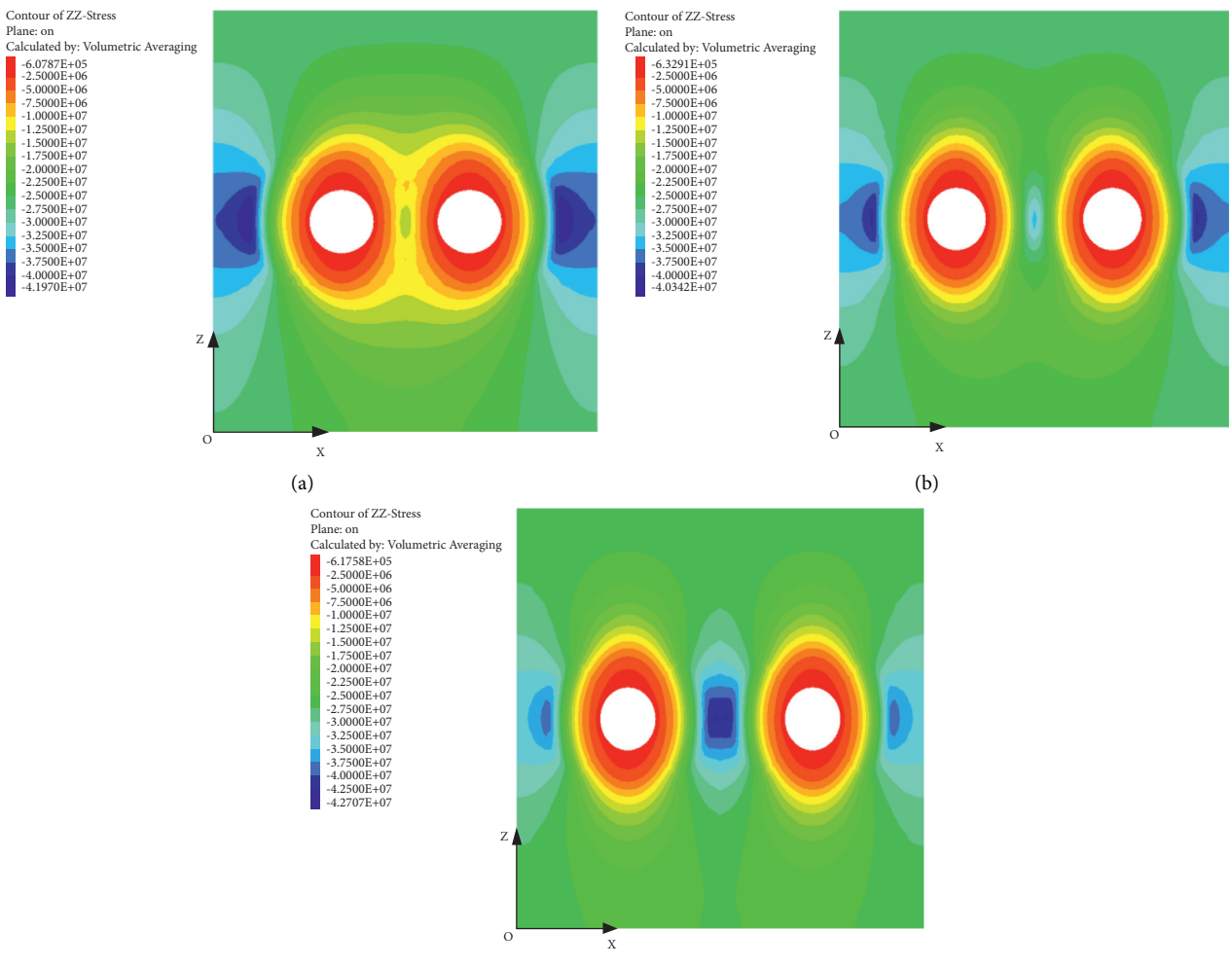


(a) (b)

(c)

Figure 15: Contour map of vertical stress around slots with different spacings in Section 1. (a) 3.0 m. (b) 4.0 m. (c) 5.0 m.

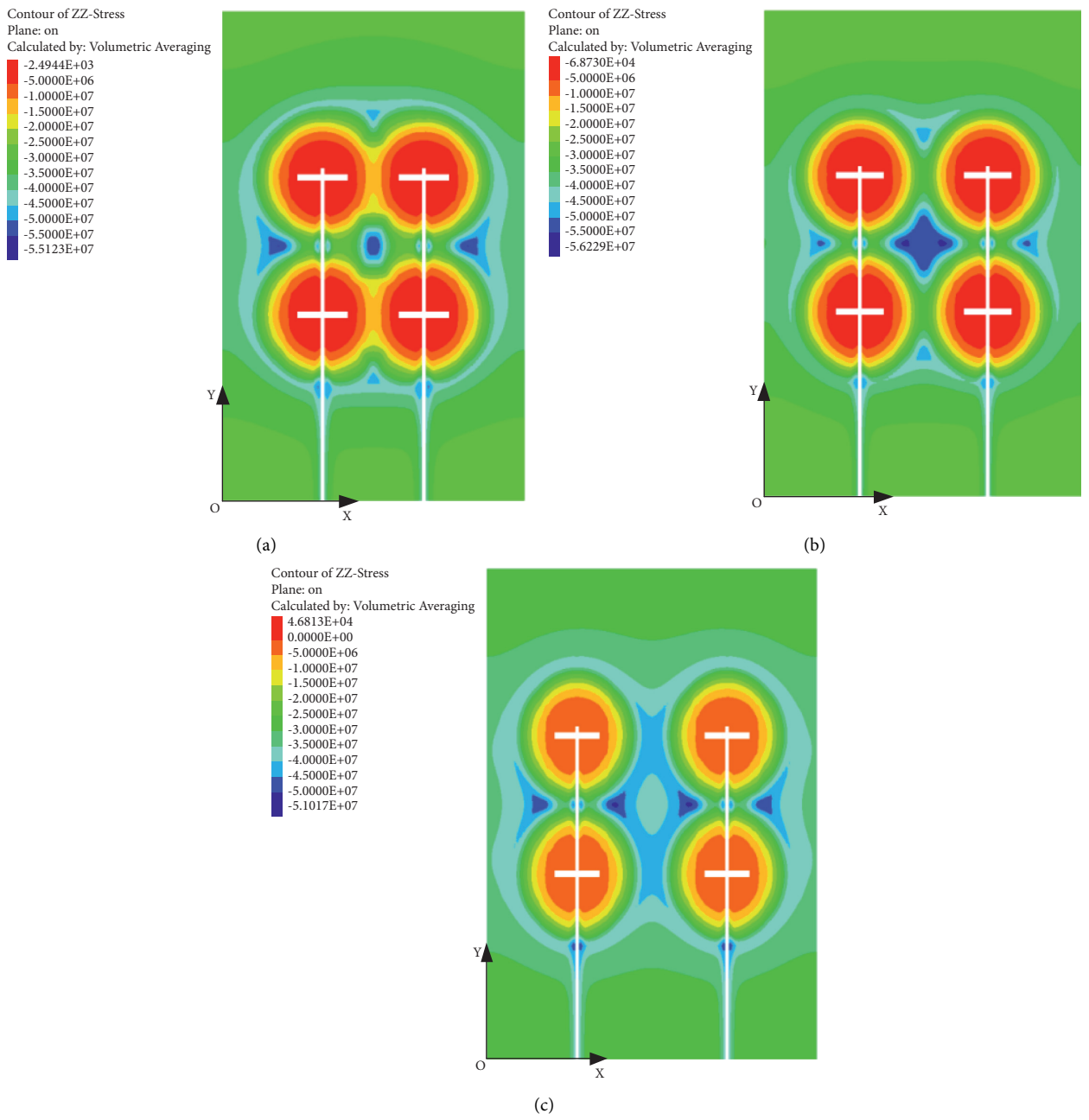


Figure 16: Vertical stress contour map around the slot with different spacings in Section 2. (a) 3.0 m. (b) 4.0 m. (c) 5.0 m.

different spacings in section 2 is shown. Figure 16 shows that the vertical stress of the "double-drilling and double-slot" model has the shape of a symmetrical "disc." According to the simulation results, when the drilling spacing is 3 m, there is only one stress concentration point with a stress of 53 MPa, between the four slots. When the drilling spacing is 4 m and 5 m, there are two stress concentration points between the four slots, with stresses of 56 MPa and 51 MPa, respectively. When the spacing is 4 m, the stress concentration degree is the highest, reaching 2.14. According to the above analysis, when the drilling spacing is 4 m or 5 m, there may be an area of original rock between the four slots, that is, the undamaged area.

(b) Plastic zone

As shown in Figures 17 and 18, the distribution of the plastic zone around the slot with different spacings in section 1 and section 2 is shown. As shown in the figures, when the spacing between drillings is 3 m, the plastic through zone is between drillings; that is, under the influence of both sides of the slot, the coal mass between boreholes is destroyed. When the spacing of drilling is 4 m,

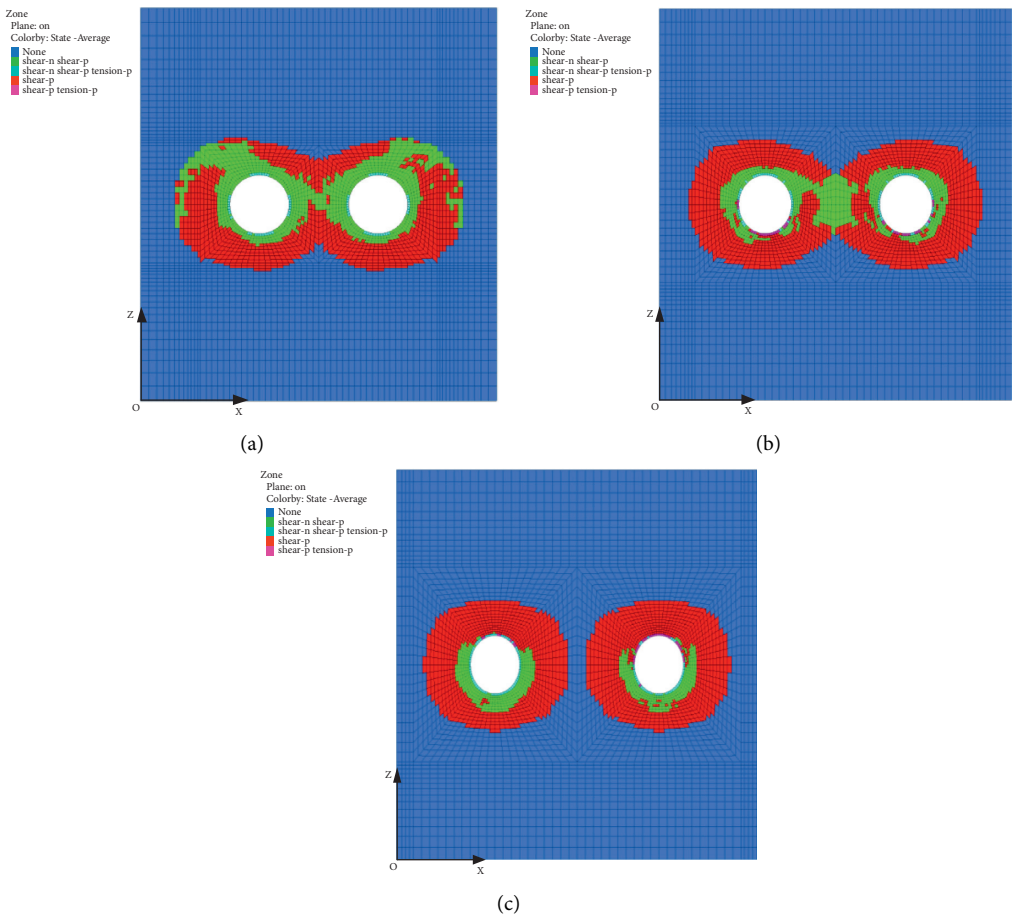


Figure 17: Distribution of the plastic zone around the slot with different spacings in Section 1. (a) 3.0 m. (b) 4.0 m. (c) 5.0 m.

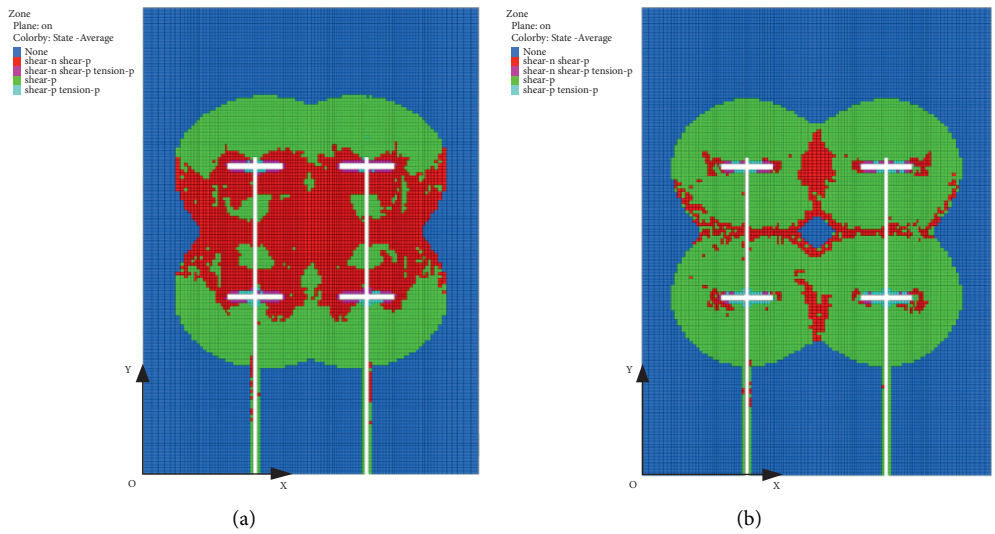


Figure 18: Continued.

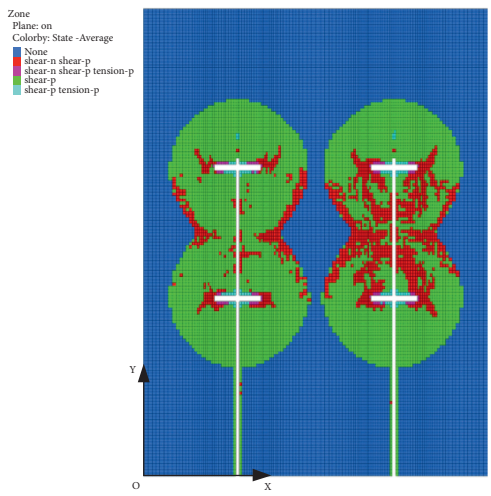


(c)

Figure 18: Distribution of the plastic zone around the slot with different spacings in Section 2. (a) 3.0 m. (b) 4.0 m. (c) 5.0 m.

there is still a plastic through zone between the drillings, but there is a certain range of original rock area between the four slots, which is smaller than that of the plastic through zone. When the distance between drillings is 5 m, the plastic through zone between drillings disappears. According to the above analysis results, the drilling spacing greatly influences the vertical stress and plastic zone between the boreholes, and with the increase in the drilling spacing, the range of the plastic zone between the drillings decreases in turn until it disappears. Therefore, considering the construction time, manpower, material resources, and other factors, it is suggested that the drilling spacing in the direction of the coal pillar length should be 3~4 m.

## 5. Field Implementation and Effect Test

### 5.1. Field Implementation

*5.1.1. Field Implementation Equipment.* The field equipment was mainly composed of a high-strength drill bit, a hydraulic slotting integral drill pipe, an ultrahigh-pressure rotating water tail, a high-pressure clean water pump, a high-low pressure conversion slot cutter, and an ultrahigh-pressure hydraulic hose (as shown in Figure 19). The equipment has good performance, a simple structure, and convenient operation.

*5.1.2. Field Implementation Process.* According to the research results in Section 4 and combined with the field conditions, a high-pressure water jet was used to destroy the residual coal pillar in the overlying goaf within 100 m of the middle section of the 38216 working face, and an ultrahigh-pressure hydraulic slotting device was placed in the design position of the 5216 roadway. According to the design scheme, workers on site drilled holes and cut seams, a total of 26 sections were arranged, and each section was set with 6 boreholes with different angles. The section spacing was 4 m. Implementation of the layout is shown in Figures 12 and 20.

The on-site construction process is as follows:

(1) The drilling rig is placed at the design position, the hydraulic slotting integral drill pipe, high-low-pressure conversion slot cutter, high-strength drill bit, and other devices are connected, the angle between the drill pipe and the roof (roadway side) is adjusted, and drilling with ordinary pressure water is performed until the design depth is reached.

(2) The ultrahigh-pressure rotating water tail is connected, the high-low pressure conversion slot cutter is placed in the set position, the water pump and the drilling rig are started, the water pressure is incrementally adjusted to 100 MPa for slotting, and the slotting time is 5 min.

(3) After cutting, the water pressure is adjusted to ordinary pressure, the 4 m drill pipe of the drilling rig is purged, and the water pressure is adjusted to 100 MPa again to continue cutting until the design scheme is completed. The field construction is shown in Figure 21.

*5.2. Effect Test.* To verify the effect of slotting, the amount of coal cinder discharged from each drilling hole and the pressure of the hydraulic support in the slotting zone are statistically analysed to verify the effectiveness and rationality of the slotting effect.

*5.2.1. Amount of Coal Cinder Discharged from Each Drilling Hole.* The hydraulic slotting pressure of each drilling hole is 100 MPa. During slotting, under the impact of a water jet and the rotation of the drill pipe, the coal blocks are discharged as small cinder particles with a diameter of 0.3~1.5 cm. As there are many boreholes on site, this part only gives the single-tool coal output of 12 boreholes on sections C and *M*, as shown in Table 4.

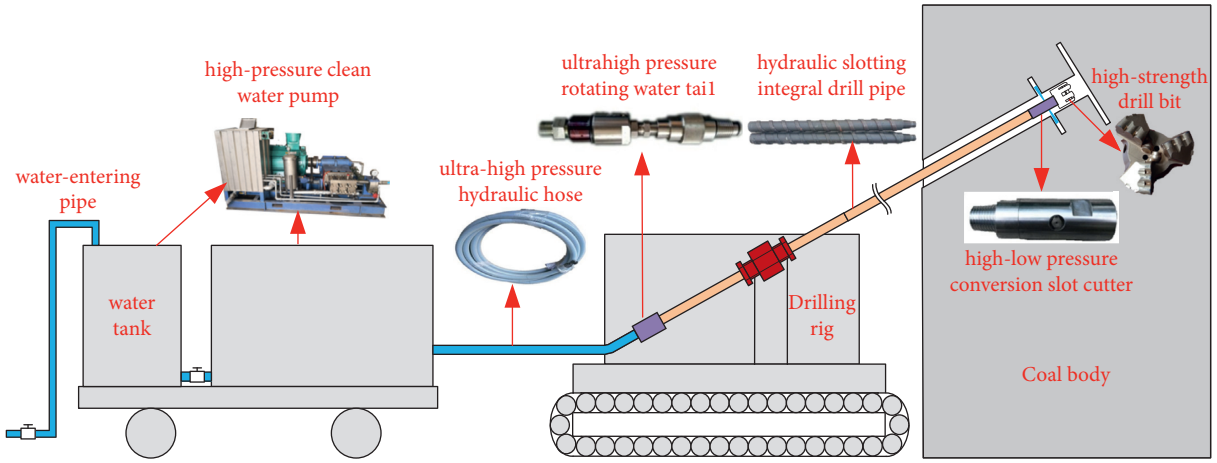


Figure 19: Ultrahigh-pressure hydraulic slotting device.

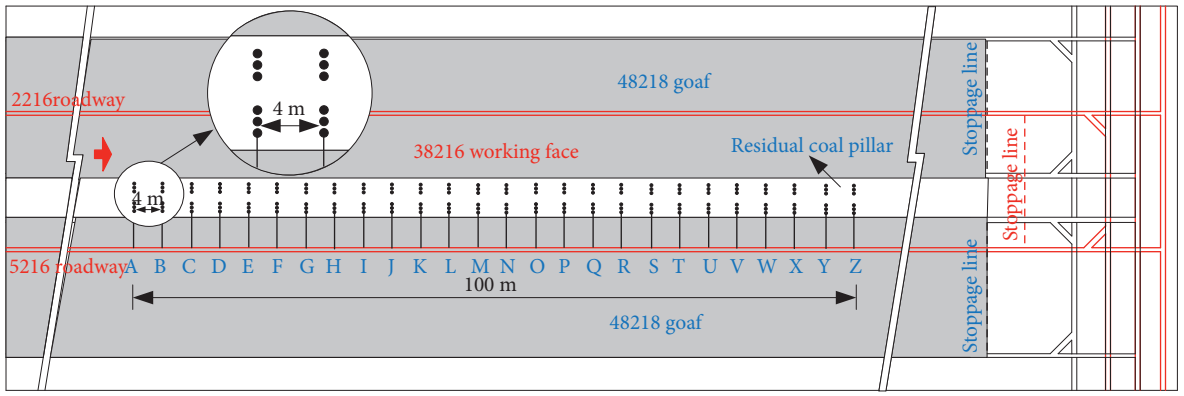


Figure 20: Layout of boreholes along the length of the residual coal pillar.

(a) (b)

Figure 21: Field construction. (a) Drilling stage. (b) Slotting stage.

Table 4: Statistics of single-drilling coal output.

| Borehole name | Single cutting time (min) | Single coal output (t) | Number of slits (time) | Total slotting time (min) | Total coal output (t) |
|---|---|---|---|---|---|
| C-1 | 5 | 0.60 | 2 | 10 | 1.20 |
| C-2 | 5 | 0.51 | 2 | 10 | 1.02 |
| C-3 | 5 | 0.57 | 3 | 15 | 1.71 |
| C-4 | 5 | 0.60 | 2 | 10 | 1.22 |
| C-5 | 5 | 0.53 | 2 | 10 | 1.06 |
| C-6 | 5 | 0.57 | 3 | 15 | 1.71 |
| M-1 | 5 | 0.51 | 2 | 10 | 1.02 |
| M-2 | 5 | 0.60 | 2 | 10 | 1.20 |
| M-3 | 5 | 0.60 | 3 | 15 | 1.80 |
| M-4 | 5 | 0.57 | 2 | 10 | 1.14 |
| M-5 | 5 | 0.60 | 2 | 10 | 1.20 |
| M-6 | 5 | 0.53 | 3 | 15 | 1.59 |

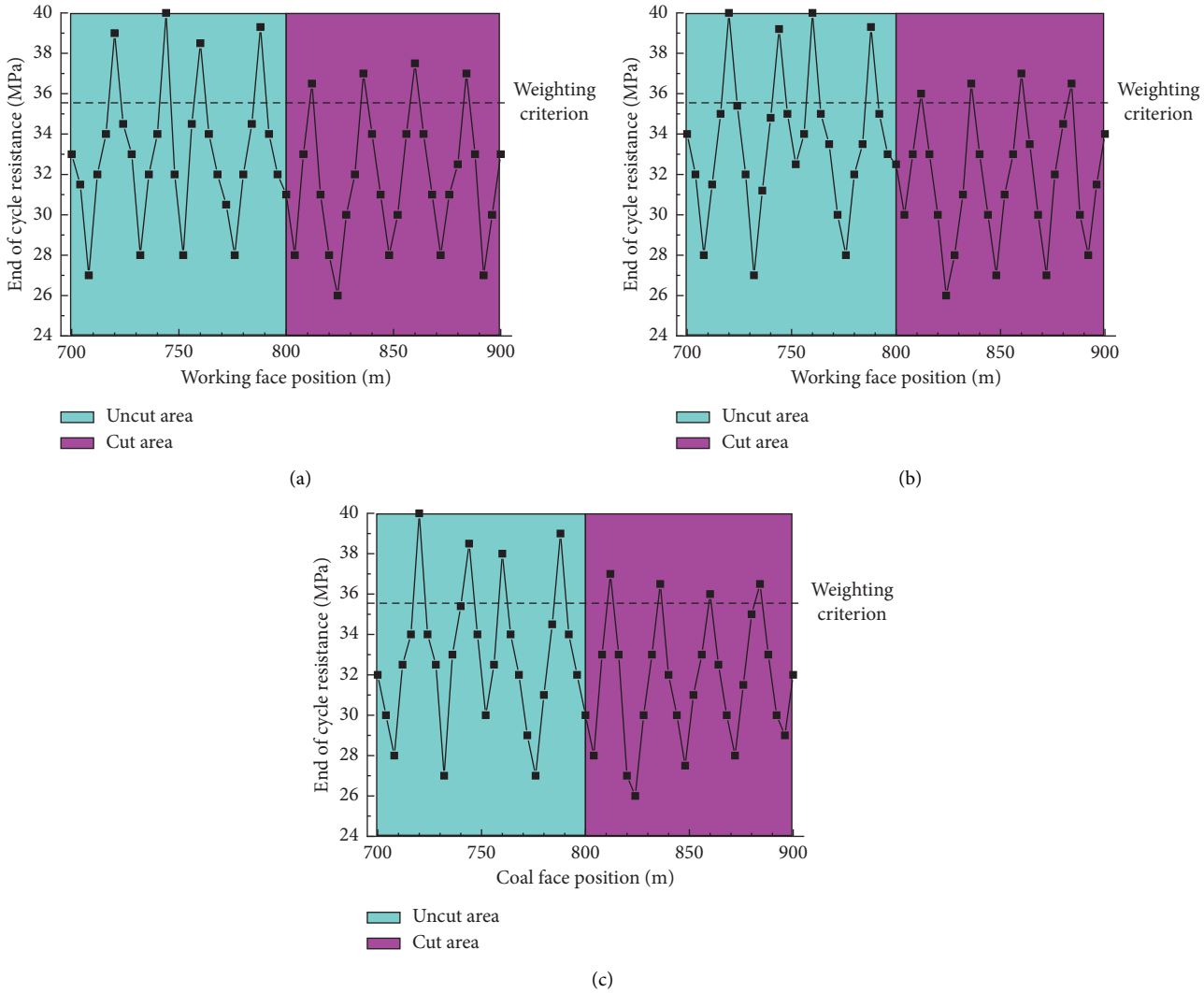


Figure 22: Data curve of typical hydraulic support under a residual coal pillar. (a) 25#. (b) 32#. (c) 39#.

$$r_c = \sqrt{\frac{M_c}{\pi h_c K_c \gamma_c}}, \tag{14}$$

Table 4 shows that at the same cutting time, the coal outputs of each drilling hole are different, approximately 0.51~0.60 t, and the average coal output of each drilling hole is 0.57 t. This may be due to the development of joints in the coal or the influence of mining, resulting in differences in the strength of coal in the same zone. Therefore, under the impact of a water jet, the single coal yield in the low-strength zone is higher, while the single coal yield in the high-strength

zone is lower.where $r_c$ is the slot radius, m; $M_c$ is the coal output of a single slot, t; $h_c$ is the slot width, m; $K_c$ is the crushing and rising coefficient of coal slag, 1.2; and $\gamma_c$ is the density of coal, t/m$^3$.

To obtain the effective radius of the slot under high-pressure hydraulic cutting, the effective radius of the slot can be deduced by the average coal output of a single slot. By substituting $M_c = 0.57$ t, $h_c = 0.2$ m, $K_c = 1.2$, and $\gamma_c = 1.41$ t/m$^3$ into equation (14), the average slot radius is approximately 0.73 m.

*5.2.2. Pressure Value of the Hydraulic Support in the Working Face.* To understand the influence of a high-pressure water jet destroying a residual coal pillar on the 38216 working face, the mine pressure behaviour of the 38216 working face was monitored, and the load change of the hydraulic support in the slotted zone and uncut zone was understood. According to the layout of hydraulic supports in the working face, there are 25 hydraulic supports (#21–46) under the residual coal pillar. Due to the large amount of data, this part gives the data curves of three typical hydraulic supports (#25, #32, and #39) under the residual coal pillar, as shown in Figure 22.

According to Figure 22, the data change trends of the three hydraulic supports are the same. In the uncut zone, the average weighting interval is 22.6 m, the working resistance is 38~40 MPa, and the maximum value is 40 MPa; in the slotting zone, the average weighting interval is 20.6 m, the working resistance is 36~37 MPa, and the maximum value is 37 MPa. The above data show that slotting has little effect on the weighting intervals and has a great influence on the variation in the working resistance of the support, and the maximum working resistance of the hydraulic support in the slotted area is reduced by 3 MPa compared with that in the uncut area. Therefore, high-pressure hydraulic slotting can reduce the working resistance of the hydraulic support under the residual coal pillar to a certain extent, which is beneficial to the safe mining of the working face.

## 6. Conclusion

Based on the geological occurrence of the No. 3 coal seam and mountain No. 4 coal seam in the Yanzishan coal mine, application of high-pressure water jet pressure relief technology to residual coal pillars in the overlying goaf of close-distance coal seams was studied by theoretical analysis and field industrial tests to provide safety guarantees and theoretical guidance for safe mining of close-distance coal seams under similar conditions. The main conclusions are as follows:

(1) According to the mine pressure and strata control and limit equilibrium theories, the elastic-plastic zone range of the residual coal pillar and the stress distribution law of the floor are obtained by structural modelling of support bearing load on the working face under the residual coal pillar, and the influence degree of the residual coal pillar on the support in the lower coal seam is revealed.

(2) Weakening the pressure of the residual coal pillar by combining high-pressure water jet and rock pressure is proposed. First, the high-pressure water jet is used to weaken the coal pillar and make the defect body in the elastic core, to destroy the coal body around the defect body, and to reduce the integrity of the coal pillar; then, yield failure of the whole coal pillar with defects is induced with mine pressure, the load transmission path of the overlying strata is cut off, and the lower close coal seam is in the low-stress zone.

(3) By establishing a mechanical model of the hydraulic cutting of a residual coal pillar and the "double-hole and double-slot" model, the high-pressure water jet drilling layout parameters are determined. The single knife cutting coal output and the hydraulic support monitoring data show that high-pressure hydraulic slotting can weaken the strength of the coal body to a certain extent, destroy the integrity of the residual coal pillar, cut off the load transmission path of the overlying strata, and reduce the working resistance of the hydraulic support under the residual coal pillar to a certain extent, which is beneficial to the safe mining of the working face.

## Data Availability

The data used to support the findings of this study are included within the article.

## Conflicts of Interest

The authors declare that there are no conflicts of interest regarding the publication of this study.

## References

[1] H. Xie, M. Gao, R. Zhang, G. Peng, W. Wang, and A. Li, "Study on the mechanical properties and mechanical response of coal mining at 1000 m or deeper," *Rock Mechanics and Rock Engineering*, vol. 52, no. 5, pp. 1475–1490, 2019.

[2] J. Lu, D. M. Zhang, G. Huang, and X. Li, "Effects of loading rate on the compound dynamic disaster in deep underground coal mine under true triaxial stress," *International Journal of Rock Mechanics and Mining Sciences*, vol. 134, no. 10, Article ID 104453, 2020.

[3] J. Ning, J. Wang, L. Jiang, N. Jiang, X. Liu, and J. Jiang, "Fracture analysis of double-layer hard and thick roof and the controlling effect on strata behavior: a case study," *Engineering Failure Analysis*, vol. 81, pp. 117–134, 2017.

[4] A. M. Suchowerska, R. S. Merifield, and J. P. Carter, "Vertical stress changes in multi-seam mining under supercritical longwall panels," *International Journal of Rock Mechanics and Mining Sciences*, vol. 61, pp. 306–320, 2013.

[5] H. Shang, J. Ning, S. Hu, S. Yang, and P. Qiu, "Field and numerical investigations of gateroad system failure under an irregular residual coal pillar in close-distance coal seams," *Energy Science & Engineering*, vol. 7, no. 6, pp. 2720–2740, 2019.

[6] J.-x. Yang, C.-y. Liu, B. Yu, and F.-f. Wu, "Calculation and analysis of stress in strata under gob pillars," *Journal of Central South University*, vol. 22, no. 3, pp. 1026–1036, 2015.

[7] C. L. Tian, X. L. Yang, H. T. Sun, Y. B. Liu, and Q. T. Hu, "Experimental study on the overburden movement and stress evolution in multi-seam mining with residual pillars," *Energy Science & Engineering*, vol. 7, no. 3, pp. 3095–3110, 2019.

[8] W. Ru, S. Hu, J. Ning et al., "Study on the rheological failure mechanism of weakly cemented soft rock roadway during the mining of close-distance coal seams: a case study," *Advances in Civil Engineering*, vol. 2020, Article ID 8885849, 20 pages, 2020.

[9] S. H. Tu, F. J. Dou, Z. J. Wang, and Y. Yuan, "Strata control technology of the fully mechanized face in shallow coal seam close to the above room-and-pillar gob," *Journal of China Coal Society*, vol. 36, no. 3, pp. 366–370, 2011.

[10] J. Z. Yang, K. G. Zheng, J. Z. Zhao, Y. J. Li, N. Dai, and H. Yang, "Research on fracturing treatment technology of concentrated stress disaster by the overlying coal pillar in close distance shallow seam," *Mining Safety & Environmental Protection*, vol. 47, no. 4, pp. 82–87, 2020, (in Chinese).

[11] B. Xia, X. Zhang, B. Yu, and J. Jia, "Weakening effects of hydraulic fracture in hard roof under the influence of stress arch," *International Journal of Mining Science and Technology*, vol. 28, no. 6, pp. 951–958, 2018.

[12] M. Behnia, K. Goshtasbi, M. F. Marji, and A. Golshani, "Numerical simulation of interaction between hydraulic and natural fractures in discontinuous media," *Acta Geotechnica*, vol. 10, no. 4, pp. 533–546, 2015.

[13] W. Y. Lu and C. C. He, "Numerical simulation of the fracture propagation of linear collaborative directional hydraulic fracturing controlled by pre-slotted guide and fracturing boreholes," *Engineering Fracture Mechanics*, vol. 235, no. 7, Article ID 107128, 2020.

[14] J. Xie, Y. P. Liang, Q. L. Zou, L. Li, and X. L. Li, "Elimination of coal and gas outburst risk of low-permeability coal seam using high-pressure water jet slotting technology: a case study in Shihuatian Coal Mine in Guizhou Province China," *Energy Science & Engineering*, vol. 7, no. 4, pp. 1394–1404, 2019.

[15] G. Si, S. Durucan, J.-Q. Shi, A. Korre, and W. Cao, "Parametric analysis of slotting operation induced failure zones to stimulate low permeability coal seams," *Rock Mechanics and Rock Engineering*, vol. 52, no. 1, pp. 163–182, 2019.

[16] Q. l. Zou, B. q. Lin, T. Liu, X. c. Hu, and C. s. Zheng, "Variations in coalbed gas content, initial gas desorption property and coal strength after drilling-slotting integration technique and gas drainage: insight into pore characteristics," *International Journal of Oil, Gas and Coal Technology*, vol. 15, no. 3, p. 235, 2017.

[17] F. Yan, B. Lin, C. Zhu et al., "A novel ECBM extraction technology based on the integration of hydraulic slotting and hydraulic fracturing," *Journal of Natural Gas Science and Engineering*, vol. 22, pp. 571–579, 2015.

[18] E. B. Yi and Y. J. Zhang, "Composite hazards prevention with breaking coal seam and roof by super high pressure water jet," *Journal of China Coal Society*, vol. 46, no. 4, pp. 1271–1279, 2021.

[19] R. Wang, J. B. Bai, S. Yan, and Z. G. Chang, "An innovative approach to theoretical analysis of partitioned width & stability of strip pillar in strip mining," *International Journal of Rock Mechanics and Mining Sciences*, vol. 129, no. 1, Article ID 104301, 2020.

[20] B. Yu, "Behaviors of overlying strata in extra-thick coal seams using top-coal caving method," *Journal of Rock Mechanics and Geotechnical Engineering*, vol. 8, no. 2, pp. 238–247, 2016.

[21] X. Zhang, C. B. Deng, and X. F. Wang, "Study on dynamic deformation of overlying strata and pressure behavior law for extraction of multiple coal seams," *Coal Science and Technology*, vol. 9, pp. 108–113, 2017.

[22] T. J. Kuang, "Study on overburden strata movement law at face end of high cutting fully–mechanized top coal caving face in ultra thick seam," *Coal Science and Technology*, vol. 6, pp. 191–196, 2016.

[23] B. Yu, R. Gao, X. B. Meng, and T. J. Kuang, "Near-far strata structure instability and associate strata behaviors in large space and corresponding control technology," *Chinese Journal of Rock Mechanics and Engineering*, vol. 37, no. 5, pp. 1134–1145, 2018.

[24] D. C. Ge, D. Li, F. X. Jiang et al., "Reasonable pressure-relief borehole spacing in coal of different strength," *Journal of Mining & Safety Engineering*, vol. 37, no. 3, pp. 578–593, 2020.